

SUPPLEMENTARY INFORMATION

Preferential survival of prebiotic metalloptides in the presence of ultraviolet light

Daniele Rossetto,^{a,b,†} Serge Nader,^b Corinna L. Kufner,^{c,§} Gabriella G. Lozano,^c Linda Cerofolini,^d Marco Fragai,^d Vlad Martin-Diaconescu,^e Barbara Zambelli,^f Stefano Ciurli,^f Graziano Guella,^g Rafał Szabla,^{h,i} Dimitar D. Sasselov,^c and Sheref S. Mansy^{*a,b}

^a DiCIBIO, University of Trento, 38123 Povo, Italy. E-mail: sheref.mansy@unitn.it

^b Department of Chemistry, University of Alberta, Edmonton, Alberta T6G 2G2, Canada.

^c Department of Astronomy, Harvard University, 60 Garden Street, Cambridge, Massachusetts 02138, USA.

^d Magnetic Resonance Centre (CERM), Consorzio Interuniversitario Risonanze Magnetiche di Metalloproteine (CIRMMP) and Department of Chemistry "Ugo Schiff", University of Florence, Sesto Fiorentino, Italy.

^e ALBA Synchrotron, Carrer Llum 2-26, Cerdanyola del Valles, Barcelona 08290, Spain.

^f Laboratory of Bio-Inorganic Chemistry (LBIC), Department of Pharmacy and Biotechnology, University of Bologna, Bologna, Italy.

^g Department of Physics, University of Trento, 38123 Povo, Italy.

^h Institute of Advanced Materials, Faculty of Chemistry, Wrocław University of Science and Technology, Wrocław, Poland.

ⁱ Department of Physics, Faculty of Science, University of Ostrava, 30. dubna 22, 701 03 Ostrava, Czech Republic.

† Current address: Synthetic Biology Group, University of Saarland, 66123 Saarbrücken, Germany.

§ Current address: Leibniz Institute of Photonic Technology, 07745 Jena, Germany.

* Sheref S. Mansy - Email: sheref.mansy@unitn.it

This PDF file includes:

- Materials and Methods
- Figures S1 to S5: Additional LC-MS and Survival data and controls
- Figure S6: potentiometric titration of GCG
- Figure S7: Metal titrations on Hook6 peptide
- Figure S8 to S12: NMR data
- Figure S13: Dissociation constants (Kd) for a library of cysteine containing peptides.
- Figure S14: Competition between Hook6 and GCG.
- Figure S15 and S16: further ITC data
- Figure S17 and S18: Affinimeter simulations
- Figure S19: UV-Vis spectra of *N*-Acetyl Cysteine Methyl Ester
- Figure S20: Absorbance difference (ΔA) spectra of *N*-Acetyl-L-cysteine methyl ester following 255 nm excitation and additional controls
- Figure S23: Analysis of EXAFS disorder parameters.
- Panel S1: EXAFS fits.
- Table S1: Peptides used in this work and Kd values
- Table S2: Parameters calculated from ITC
- Table S3: Vertical excitations energies of the model peptide coordinating Zn²⁺ cations

Materials and Methods

Peptide synthesis. Peptides were synthesized via solid phase peptide synthesis, as previously described¹. *N,N*-dimethyl formamide (DMF) was used as the solvent and Wang resin (Fmoc-Gly-Wang) was used as the starting polymeric support. Trityl-protected Fmoc-cysteine (Fmoc-Cys(Trt)-OH) and tert-butyl (OtBu) side chain-protected Fmoc- α -amino acids were used as the building blocks. The peptide chain was elongated by sequential Fmoc deprotection of the residue anchored to the resin and Fmoc-AA-OH coupling. Fmoc deprotection was obtained by washing the mixture with 20% (v/v) solution of piperidine in DMF. For each coupling, an excess (Fmoc-AA-OH: anchored AA, 4:1) of the Fmoc- α -amino acid derivative was added to the resin. Apart from Fmoc-Cys(Trt)-OH, Fmoc- α -amino acid derivatives were activated with a mixture of hydroxyl-benzotriazole (HOBt), *N,N,N',N'*-tetramethyl-O-(benzotriazol-1-yl)uronium tetrafluoroborate (TBTU), and *N,N*-diisopropylethyl amine (DIPEA). Fmoc-Cys(Trt)OH was activated with a *N,N'*-diisopropylcarbodiimide (DIC)/HOBt mixture with a *N,N'*-diisopropylcarbodiimide (DIC)/HOBt mixture. At the end of the synthesis, the polymers were cleaved from the resin and deprotected by treatment with a solution of trifluoroacetic acid (TFA):H₂O:triisopropyl silane (TIS):1,2-ethanedithiol (EDT) (97:1:1:1, v/v) for 2 h. The product was precipitated with cold diethyl ether/petroleum ether (30:70, v/v) followed by washing cycles with diethyl ether. The peptides were finally solubilized in 20% acetic acid (v/v), flash frozen in liquid nitrogen and lyophilized overnight at -84 °C (Labconco FreeZone Freeze Dryer).

Design of Zinc Hook peptides. Hook peptide designs were inspired by Kočańczyk et al.² The zinc hook region of their Rad50 protein in which Arg449 was exchanged with Ala was used to generate the sequence of Hook₁₄ (AKGKCPVCGAELTD). Hook₆ was designed by removing the regions flanking the core of the metal-binding site, i.e. the sequence was KCPVCG.

Affinity measurements. Solutions of peptide were prepared by dissolving the peptides in 20 mM Gly-Gly, pH 8.7 inside a glovebox to a total thiol concentration 5 mM. Degassed LC-MS water was used throughout the experiments. UV-vis spectra of the samples were recorded inside a glovebox with a Genesys 150 UV-Vis spectrophotometer (ThermoFisher) with an integration time of 0.5 s and an interval of 1 nm. Spectra were collected after each addition of metal and the absorbance at 750 nm, typical of a tetrathiolate-Co²⁺ complex, was fit with GraphPad Prism v. 6.00 (GraphPad Software, La Jolla California USA) to the following equation: $y = B_{\text{Max}} \cdot x^h / (K_{\text{d}} + x^h)$, where B_{Max} was the absorbance reached at saturation and h was the Hill slope. To overcome the spectroscopic silence of Zn(II), competitive binding experiments involving a preformed peptide-Co(II) complex, where the characteristic absorbance at 750 nm was exploited. A decrease in the absorbance at 750 nm was observed upon titration

with Zn^{2+} . The concentration of Co(II) added to each peptide before the competition assay was coincident with the K_d value of that complex. UV-vis spectra were collected upon each addition. Titrations continued until no changes in absorbance at 750 nm were observed. The K_d values for the zinc(II) complexes were calculated by fitting to a revised Cheng-Prusoff equation, as previously described³.

UV irradiation. Peptides were dissolved under anoxic conditions in aqueous 20 mM glycylglycine to a final thiol concentration of 5 mM, and the pH adjusted to 8.7, unless indicated otherwise. Metal ions were added to the solution from a 333.3 mM solution and transferred to a sealed high-quality quartz Hellma cuvette. Samples were extracted from the glovebox and irradiated with a Rayonet RPR-200 reactor with sixteen 14 W light sources with an approximate photon flux of 1.65×10^{15} $F\lambda$ [$cm^{-1} s^{-1}$] at 253.7 nm (15 nm window), which was 4000-fold greater than that of the prebiotic sun at 254 nm. Therefore, every minute of irradiation in the reactor corresponded to ~7 days of continuous irradiation on the prebiotic Earth. 4,422 h of light per year at the equator was used to convert lifetimes.

LC-MS analysis. 2.5 μ L aliquots were either analyzed with a Shimadzu HPLC system (CBM-20 A, binary pump LC-20AB) or an Agilent 1260II HPLC with an Infinity iQ Mass Selective Detector. Runs on the Shimadzu system used a Kinetex C18 column (100 Å pore size, 4.6 mm ID, 2.6 μ m particle size, 25 cm length, Phenomenex). The mobile phase was composed of Solvent A (0.1% trifluoroacetic acid (TFA) in LC-MS grade water) and Solvent B (0.1% TFA in acetonitrile) and a gradient from 1% (vol/vol) solvent B to 20% (vol/vol) solvent B in 20 min. Data were acquired with LabSolutions LC software. Runs on the Agilent system used a Zorbax SB-Aq column (80 Å pore size, 4.6 mm ID, 1.8 μ m particle size, 15 cm length, Agilent) and a gradient from 100% solvent A for 6 min to 100% solvent B in 20 min. Data were acquired with OpenLab 2.5 software. MS measurements were carried out in ESI-positive ion mode. Half-life values were obtained by fitting the data to a delayed one-phase decay model (equation: $y=(y_0-p)*e^{(-k(x-x_0))} + p$) with GraphPad Prism v. 6.00 (GraphPad Software, La Jolla California USA), where y_0 is the survival at t_0 , p is the survival at infinite time, x_0 is the time at which the decay begins, and k is the rate constant. All experiments were in triplicate.

Isothermal Titration Calorimetry. Peptide solutions were prepared with degassed LC-MS grade water and stored in anaerobic conditions until the experiments were performed. The solutions included 2.5 mM Gly-Gly (GG) buffer and 300 μ M tris(2-carboxyethyl)phosphine hydrochloride (TCEP) and were adjusted to pH 8.7. Metal ions and peptide titrations were performed at 25 °C using a high-sensitivity VP-ITC microcalorimeter (MicroCal LLC, Northampton, MA). The reference cell was filled with deionized water. Each experiment was started with a small injection of 1–2 μ L, which

was discarded from the analysis of the integrated data to avoid artifacts due to diffusion through the injection port occurring during the long equilibration period, locally affecting the peptide concentration near the syringe needle tip. Care was taken to start the first addition after baseline stability had been achieved. In each individual titration, small volumes (5–10 μL) of a solution containing ZnSO_4 , at a concentration of 750 - 2000 μM were injected into a solution of peptide using a computer-controlled 310- μL microsyringe. To allow the system to reach equilibrium, we applied a spacing of 300–360 s between each injection of ligand. A control experiment was set up, titrating the metal solution into the buffer alone, under the same conditions. Integrated heat data were obtained for Zn^{2+} titrations using NITPIC software⁴ and were fit with a nonlinear least-squares minimization algorithm to a theoretical titration curve, using the MicroCal Origin software. ΔH (reaction enthalpy change in cal mol^{-1}), K_a (binding constant in M^{-1}), and n (number of binding sites) were the fitting parameters. The reaction entropy was calculated using the relationships $\Delta G = -RT \ln K_b$ ($R = 1.9872 \text{ cal mol}^{-1} \text{ K}^{-1}$, $T = 298 \text{ K}$) and $\Delta G = \Delta H - T\Delta S$. The values given for ΔH and ΔS are apparent and include contributions, not only from metal binding, but also from associated events such as protonation/deprotonation of the amino acid residues involved in the binding and consequent change in the buffer ionization state. The reduced chi-square parameter χ^2_v ($\chi^2_v = \chi^2/n$, where n is the degrees of freedom, $n = N_{\text{idp}} - N_{\text{par}}$, N_{idp} = number of points, and N_{par} = number of parameters floating in the fit) was used to establish the best fit. Best fits were obtained using the one set of sites with ligand in the cell model.

X-Ray Absorption Spectroscopy. Aqueous solution samples consisting of 5 mM metal (Zn^{2+}) mixed with the tripeptide GCG at concentrations of 5 mM, 10 mM, and 20 mM total thiol were prepared anaerobically and loaded into the sample holders. Data were collected at liquid nitrogen temperatures (80 K), in fluorescence mode employing a Si311 double crystal monochromator and a 6 channel multi-element SDD detector available at the ALBA synchrotron, CLAEISS beamline. Data was averaged, normalized and calibrated using the Athena software package.⁵ Zn K-edge energies were calibrated to the first inflection point of Zn metal foils taken as 9659 eV. EXAFS spectra were extracted using the autobk algorithm with a spline in the 0 to 13.8 \AA^{-1} region having an R_{bkg} of 1. EXAFS fitting of the data was carried out with Larch, the python implementation of Artemis.^{6,7} The FEFF6 code^{7,8} was used for scattering path generation, and multi (k^1 , k^2 , k^3)-weighted fits of the data were carried out in r -space over an r -range of 1 to 2.3 \AA and a k -range of 2.5-12.0 \AA^{-1} . The S_0^2 value was set to 0.9, and a global E_0 was employed with the initial E_0 value set to the inflection point of the rising edge. Single scattering paths were fit in terms of a Δr_{eff} and σ^2 . To assess the goodness of the fits, both the R_{factor} (%R) and the reduced χ^2 (χ^2_v) were minimized, ensuring that the data were not over-fit. For the latter, a drop by a factor of $1 + \sqrt{2/v}$ was ensured when considering an increasing number of variables.⁹

Picosecond TA Measurements. The TA measurement was conducted on a Helios Fire (Ultrafast Systems, LLC) system (general concepts of pump-probe spectroscopy are explained in the literature, e.g. ¹⁰). As light source, a Ti:Sa based oscillator/ regenerative amplifier system (Solstice Ace, Spectra Physics: 800 nm wavelength, ~7 mJ output energy, 1 kHz repetition rate, ~100 fs pulse duration) was used to generate both pump and probe pulses (continuum within Helios Fire). The 255 nm pump pulses were generated by conversion of the 800 nm output pulses via an optical parametric amplifier system (Topas Prime + NirUVis, Spectra Physics). Afterwards, the pump pulses were stretched to ~1.5 ps by a 25 cm long UV fused silica block (Corning, USA) to reduce 2-photon excitation of both the solvent and sample and chopped to 500 Hz. Both pump and probe pulses were focused on the sample (190 μm x 300 μm pump, 130 μm x 220 μm probe at a 90:10 level) under 54.7 ° polarization conditions (magic angle). The energy of the excitation pulses at the sample position was ~0.22 μJ . The TA spectra were recorded in the delay interval between -5 ps and 7 ns in 5 scans from low to high delays with an averaging time of 4 s per delay position over a total measurement time of 30 min. The results are shown in Figure 6B and Figure S20. The excitation conditions were chosen carefully to minimize the overlapping background signal from solvated electrons due to 2-photon-excitation of the aqueous solvent (Figure S21). As control, blank LC-MS grade water and an adenosine monophosphate (AMP) solution with the same absorbance as the sample at 255 nm (vertical line in Figure 6A) were measured under identical conditions (Figure S21). From this, the solvated electron background signal was determined to be ≤ 0.1 mOD. As a concentration control, UV / Vis spectra in the range between 200 nm and 360 nm were taken before and after each scan (every 6 min) of the transient absorption (TA) measurements (Figure S22 showing the wavelength range 200 nm to 300 nm). During the TA measurement, the absorbance of the *N*-Acetyl-L-cysteine methyl ester was kept within $\leq 7\%$ of the starting absorbance (Figure S22).

Excited-state quantum-chemical calculations. We constructed the initial geometries of the glycine-cysteine-glycine tripeptides with and without the zinc atom using the MOLDEN¹¹ and Avogadro¹² programs. The ground state geometries were optimized using the range separated CAM-B3LYP DFT approximation¹³ including the empirical D3 dispersion correction with Becke-Johnson damping. We used the def2-TZVP triple-zeta basis set for the DFT calculations and the conductor-like continuum solvation model of bulk water (C-PCM). To speed up the Fock-exchange part of the DFT calculations, the chain of spheres approximation (RIJCOSX) was applied.¹⁴ For excited-state calculations we used the algebraic diagrammatic construction to the second order [ADC(2)]^{15,16} method and the TZVP basis set. We also used the COSMO solvation model of bulk water to mimic the solvation effects for the ADC(2) calculations.¹⁷ We applied the non-equilibrium variant of the COSMO solvent model to calculate the vertical excitation energies. The solvent was equilibrated for the S_1 electronic state, during the excited-state geometry optimizations of S_1 minima.¹⁷ Similarly, the equilibrium variant of the COSMO model was used for the calculation of the excited-state potential energy profile

also involving the ADC(2)/TZVP method. The excited-state potential energy profile was calculated using two approaches. First, we performed a linear interpolation in internal coordinates (Z-matrices) between the ground-state geometry (Frank-Condon region) and the S_1 minimum-energy structure. Next, starting from the S_1 minimum, we performed a relaxed scan for the O...H distance that is the primary reaction coordinate of the electron-driven proton transfer mechanism

NMR measurements. 2D NMR experiments for resonance assignment (2D ^1H - ^{15}N -HSQC, 2D ^1H - ^{13}C -HSQC, 2D ^1H - ^1H -TOCSY, 2D ^1H - ^1H -COSY and 2D ^1H - ^1H -NOESY, mixing time: 120 ms) were performed on solutions of Hook₆ and Hook₁₄ at the concentration of 15 mM in the presence of Zn^{2+} . The spectra were recorded on a Bruker AVANCE NEO spectrometer operating at 16.4 T (700 MHz ^1H Larmor Frequency), equipped with a triple resonance cryoprobe. Additional 2D ^1H - ^1H -NOESY experiments at different mixing times (120, 200, 300 ms) were recorded on the sample of Hook₁₄ peptide using a Bruker AVANCE III spectrometer, operating at 22.3 T (950 MHz ^1H Larmor Frequency). All the spectra were acquired at 298 K, processed using Topspin (version 4.0) and analyzed with CARA (Keller, R., Cantina Verlag, 2004). NMR assignment of Hook₁₄ was performed starting from the analysis of 2D ^1H - ^1H -TOCSY and ^1H - ^1H -COSY spectra, to identify the residue spin systems. Then the analysis of 2D ^1H - ^{13}C HSQC and 2D ^1H - ^{15}N HSQC spectra allowed for the assignment of the carbon and nitrogen resonances, respectively, and confirm the residue types. Analysis of 2D ^1H - ^1H -NOESY allowed us to obtain residue-sequential connectivity and long-range correlations.

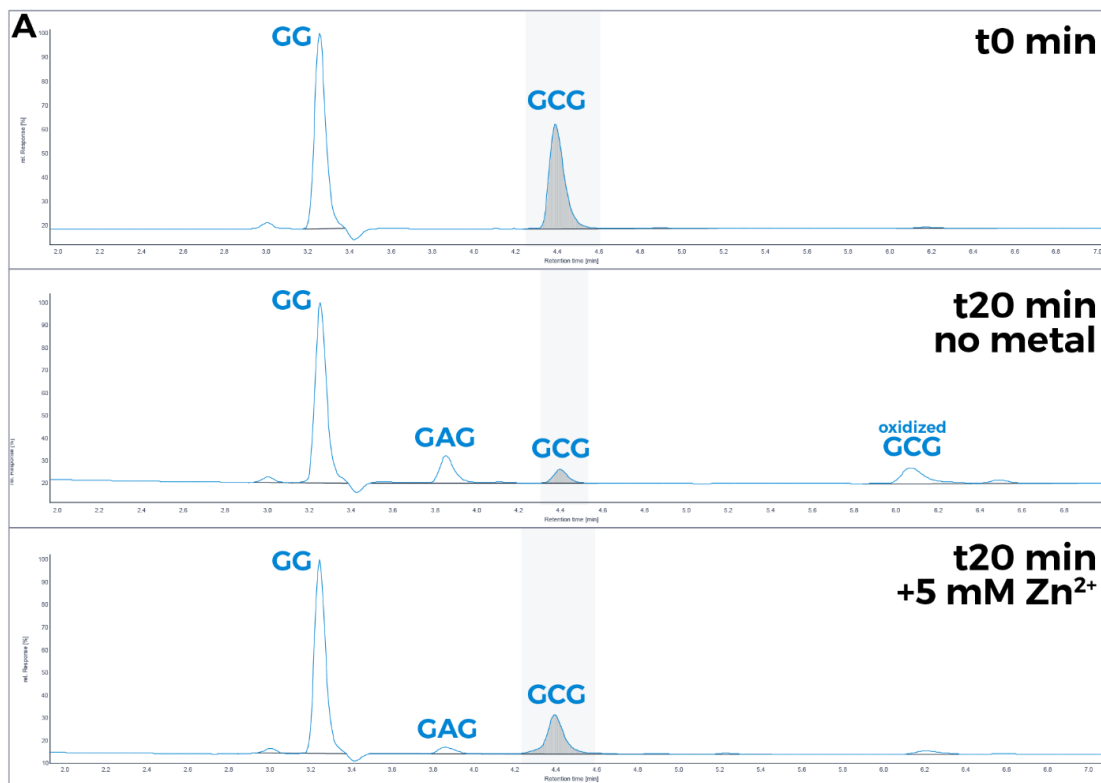


Figure S1: Degradation of GCG peptide upon UV irradiation monitored by LC-MS. Chromatographic runs of 5 mM GCG in 20 mM Glycylglycine at pH 8.7, upon irradiation at 254 nm for 20 min in absence or presence of 5 mM Zn²⁺. Assignments were consistent with the values of isotopic mass calculated for the protonated molecules [M+1]. M/z of the detected species: GCG=236.0 Da, GAG=204.1 Da, GG=133.0, oxidized GCG=469.1 Da.

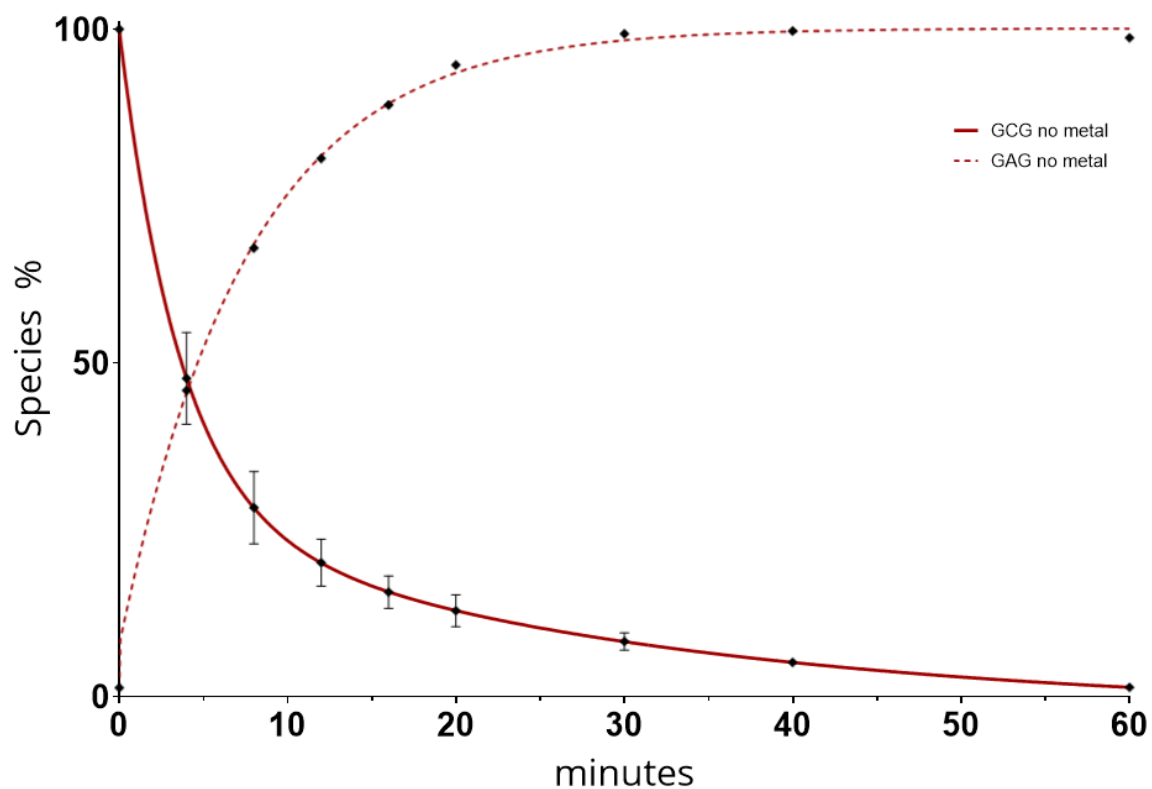


Figure S2: Degradation of GCG peptide and conversion to GAG upon UV irradiation monitored by LC-MS. Degradation of 5 mM GCG peptide over time in absence of metal ions (solid line) and conversion into GAG species (dotted line). Data points were fitted to a one-phase decay model. Data are mean \pm SD; n = 3

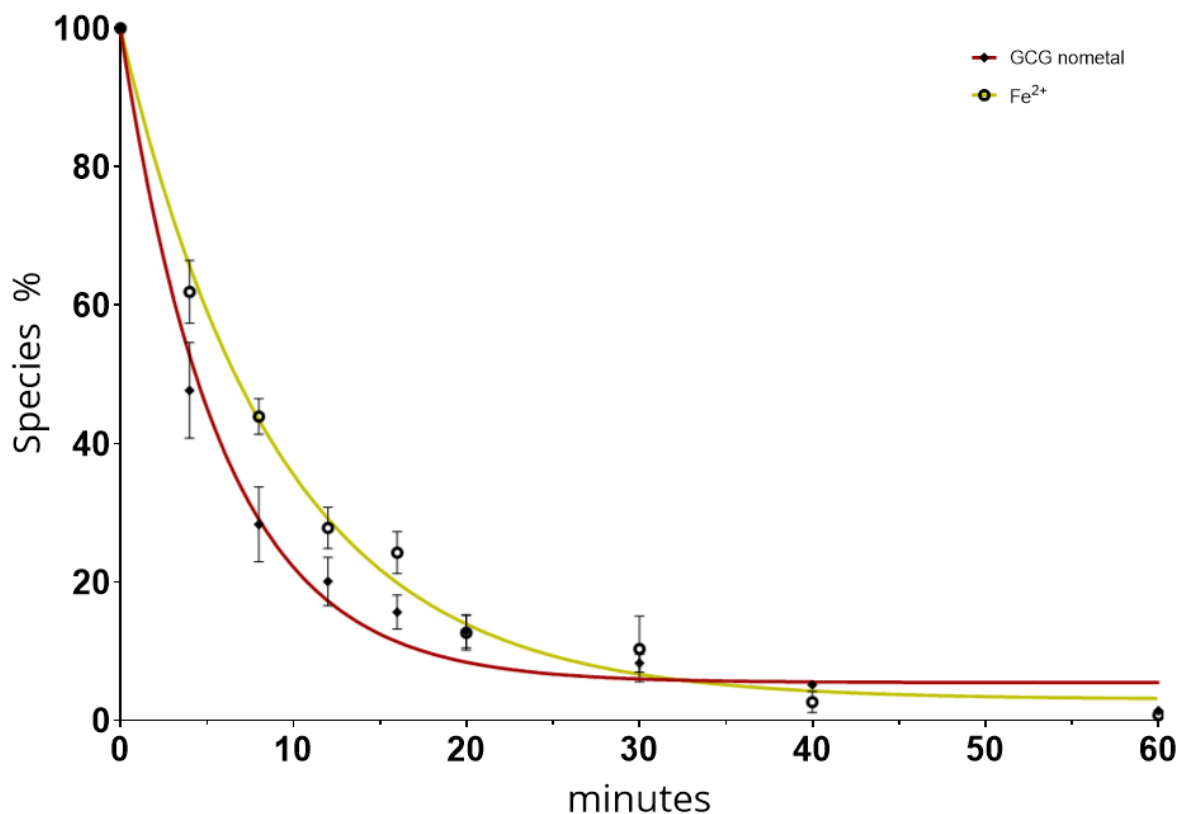


Figure S3: Degradation of GCG peptide upon UV irradiation monitored by LC-MS. Degradation of 5 mM GCG peptide over time in buffer conditions only and in presence of 5 mM Fe²⁺. Data points were fitted to a one-phase decay model. Data are mean \pm SD; n = 3.

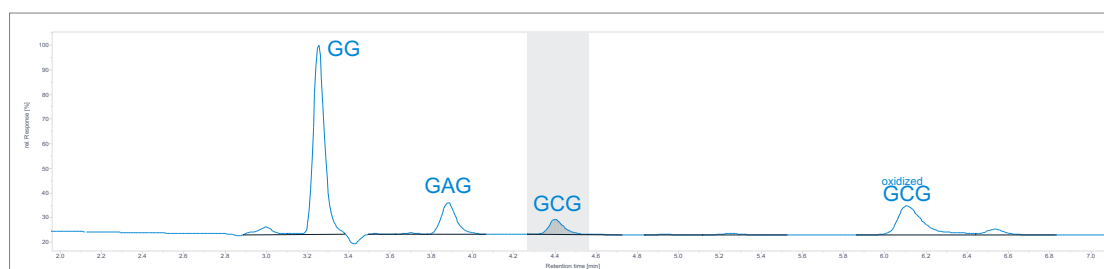


Figure S4: Degradation species of GCG peptide upon UV light in presence of Fe²⁺. Chromatographic runs of 5 mM GCG in 20 mM Glycylglycine buffer at pH 8.7, upon 20 min irradiation at 254 nm in presence of 5 mM Fe²⁺. Assignments were consistent with the values of isotopic mass calculated for the protonated molecules [M+1]. M/z of the detected species: GCG=236.0 Da, GAG=204.1 Da, GG=133.0, oxidized GCG=469.1 Da.

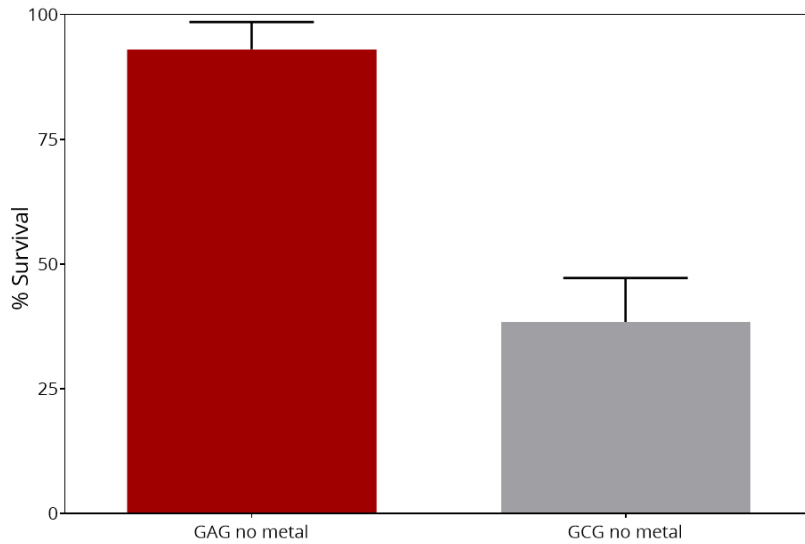


Figure S5: GAG survival upon UV irradiation. 5 mM GAG peptide in 20 mM GG at pH 8.7 was irradiated at 254 nm for 8 min. Data are mean \pm SD; n = 3.

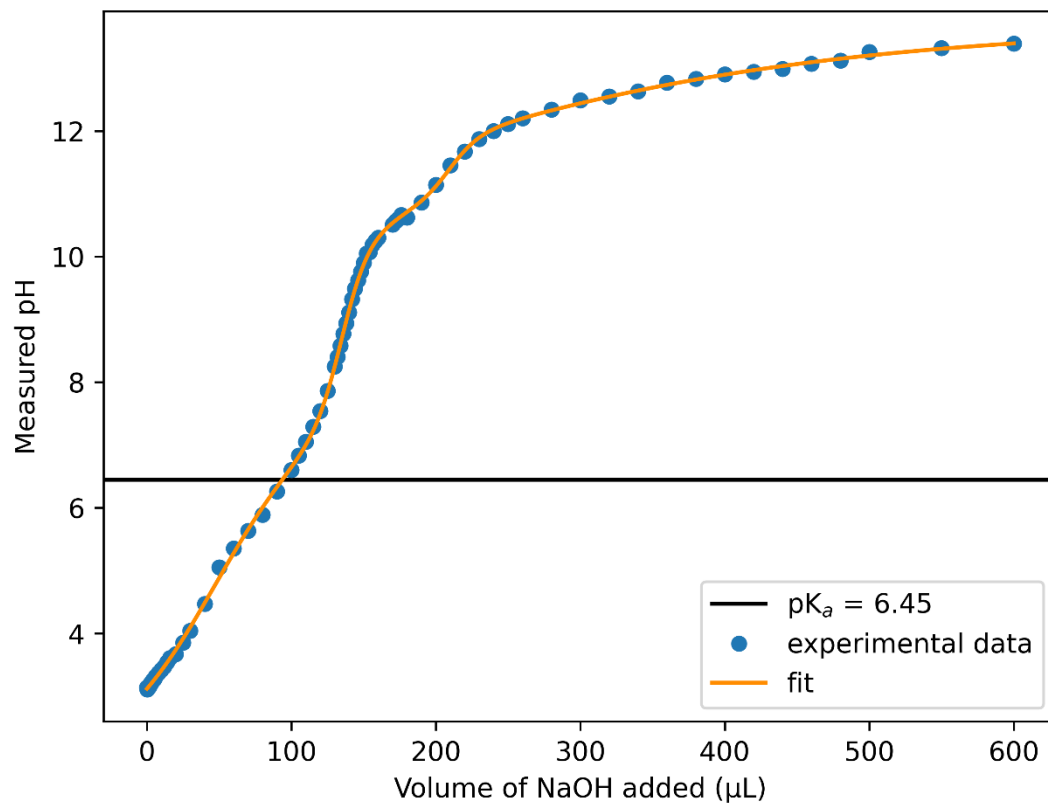


Figure S6: potentiometric titration of 10 mM GCG in presence of 2.5 mM Zn^{2+} . The black line identifies the calculated $pK_a = \sim 6.45$.

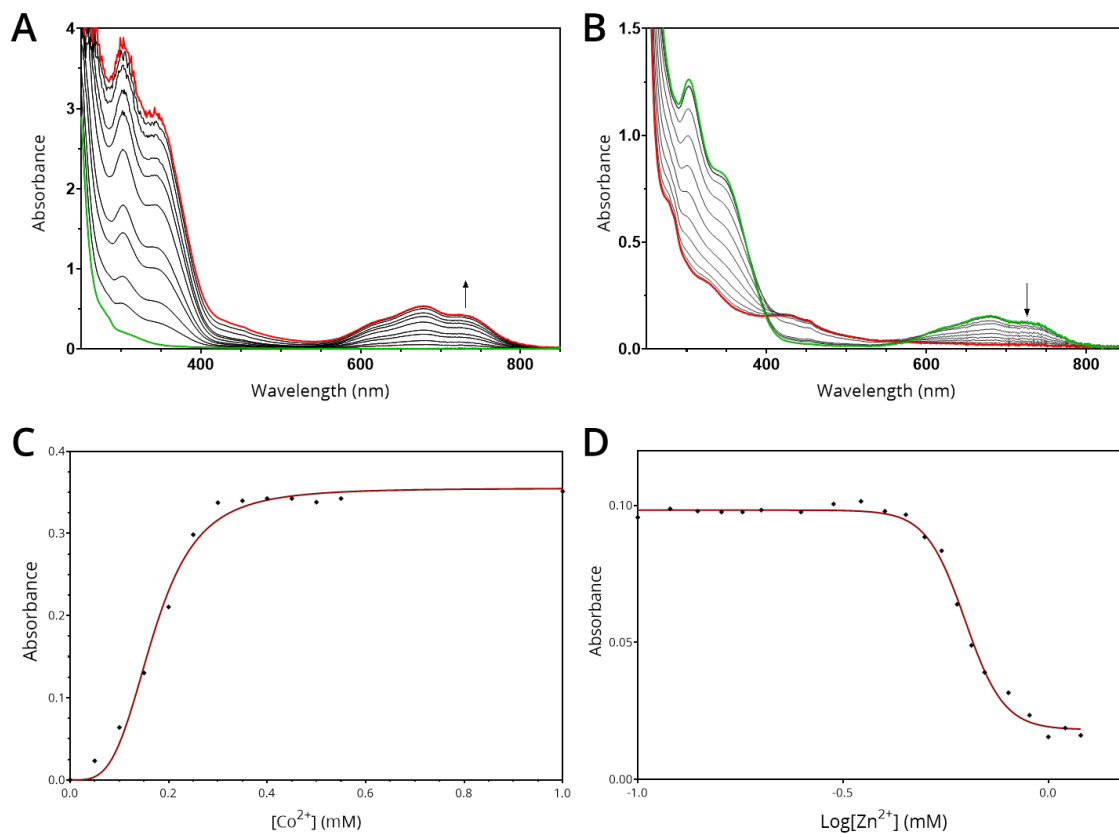


Figure S7: Co²⁺ and Zn²⁺ titration experiments of 2.5 mM Hook₆ peptide in 20 mM GG at pH 8.7. A: titration of Hook₆ peptide with Co²⁺. B: Titration of pre-formed peptide-Co²⁺ complex with Zn²⁺. C: Saturation binding curve of Hook₆ peptide in the presence of Co²⁺. D: Competition binding curve of pre-formed Hook₆-Co²⁺ complex.

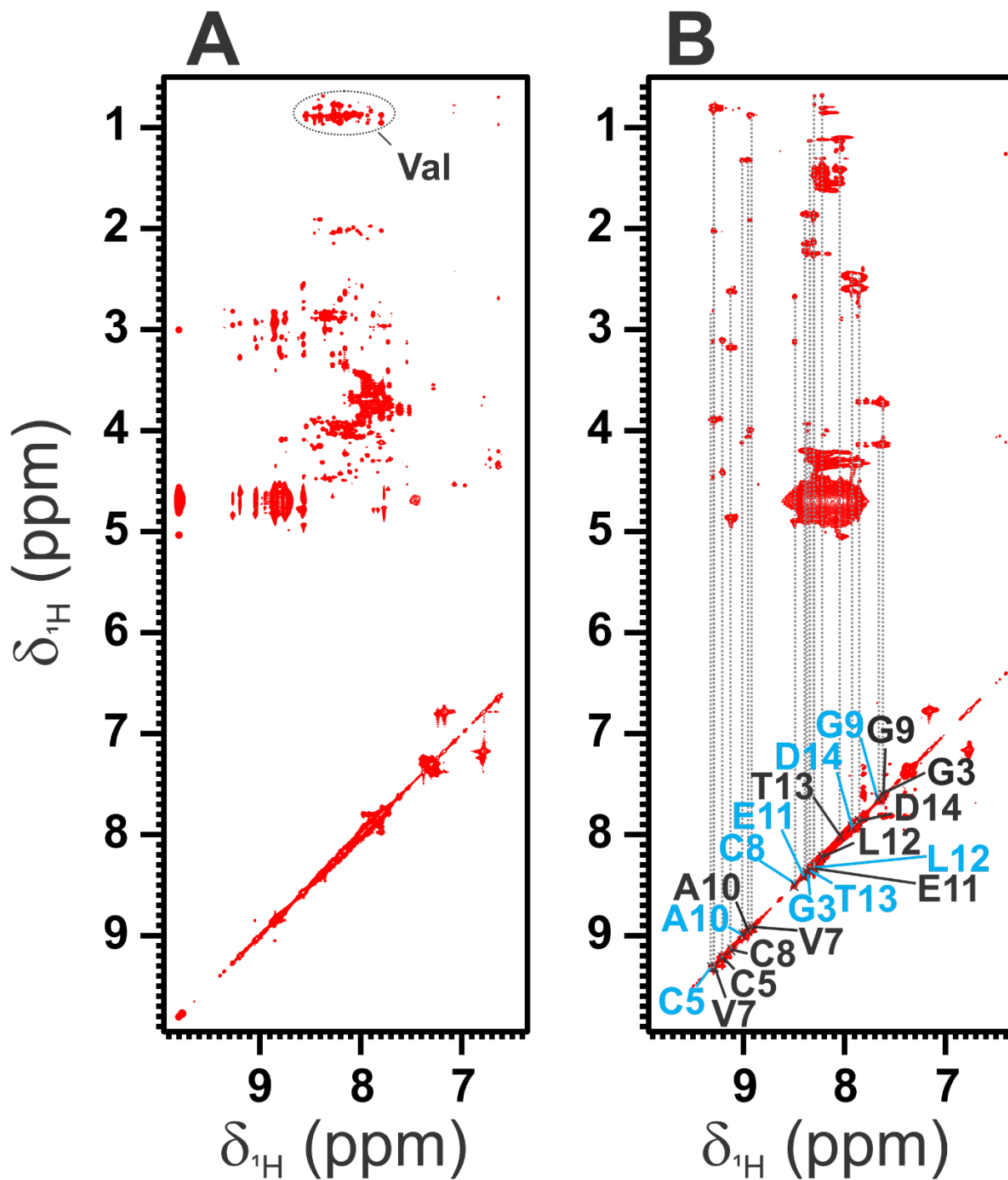


Fig. S8: H_N region of the 2D 1H - 1H -TOCSY solution NMR spectra of A) Hook₆ and B) Hook₁₄. The spin systems assigned to the two different species in the spectrum of Hook₁₄ are labeled in black and cyan, respectively. The spectra were recorded at 298 K on a Bruker AVANCE NEO spectrometer operating at 16.4 T (700 MHz 1H Larmor Frequency), using water solutions (90% H₂O, 10% D₂O) of the peptides at 15 mM, in the presence of Zn(II) metal ion.

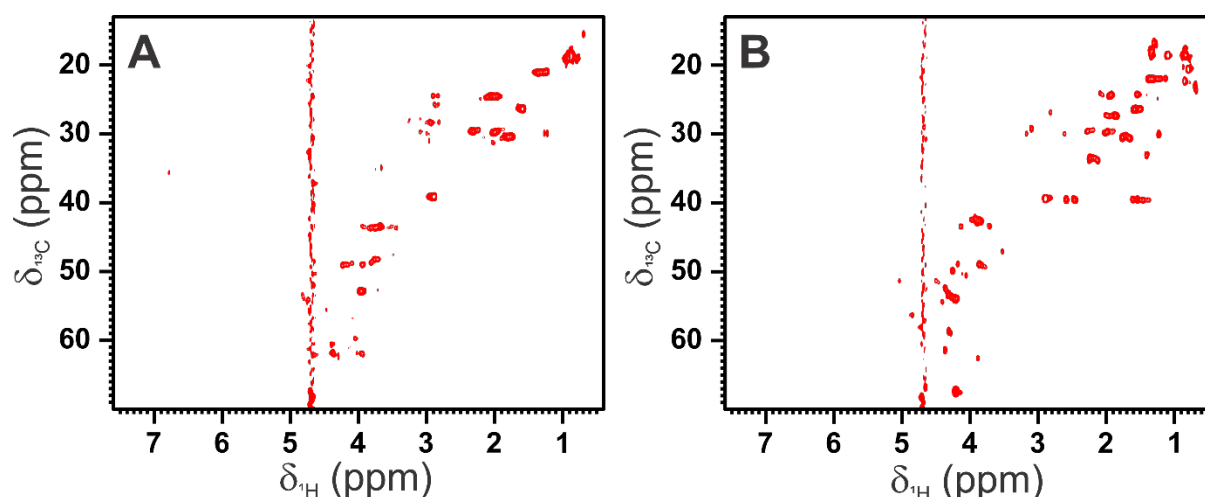


Fig. S9: 2D ^1H - ^{13}C -HSQC NMR spectra corresponding to A) Hook₆ and B) Hook₁₄. The spectra were recorded at 298 K on a Bruker AVANCE NEO spectrometer operating at 16.4 T (700 MHz ^1H Larmor Frequency), using water solutions (90% H_2O , 10% D_2O) of the peptides at 15 mM, in the presence of Zn(II) metal ion.

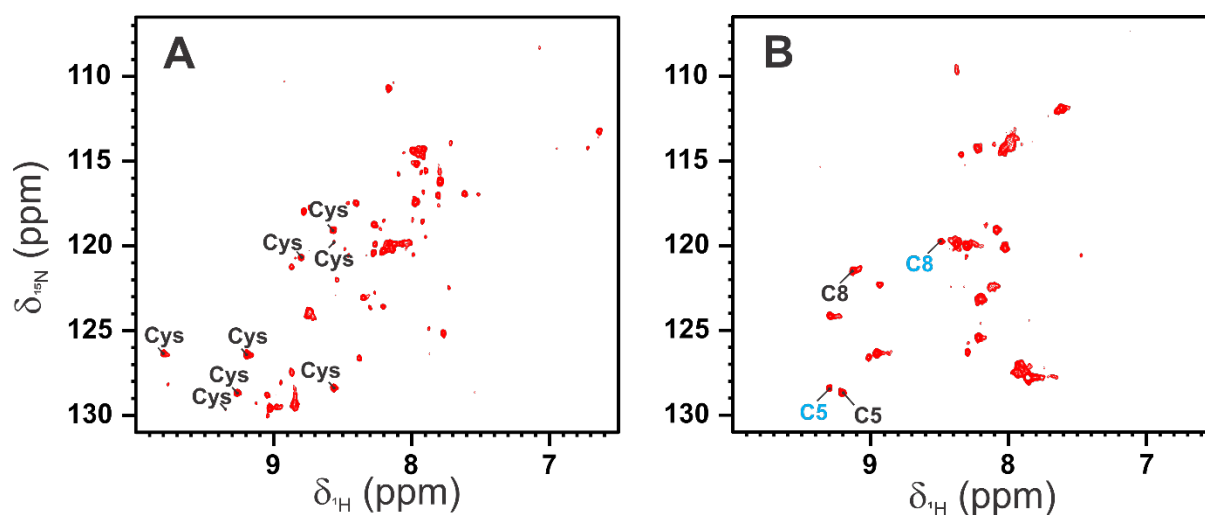


Fig. S10: 2D ^1H - ^{15}N -HSQC NMR spectra corresponding to A) Hook₆ and B) Hook₁₄. The cross-peaks assigned to cysteine residues are labeled. The spin systems assigned to the two different species in the spectrum of Hook₁₄ are labeled in black and cyan, respectively. The spectra were recorded at 298 K on a Bruker AVANCE NEO spectrometer operating at 16.4 T (700 MHz ^1H Larmor Frequency), using water solutions (90% H_2O , 10% D_2O) of the peptides at 15 mM, in the presence of Zn(II) metal ion.

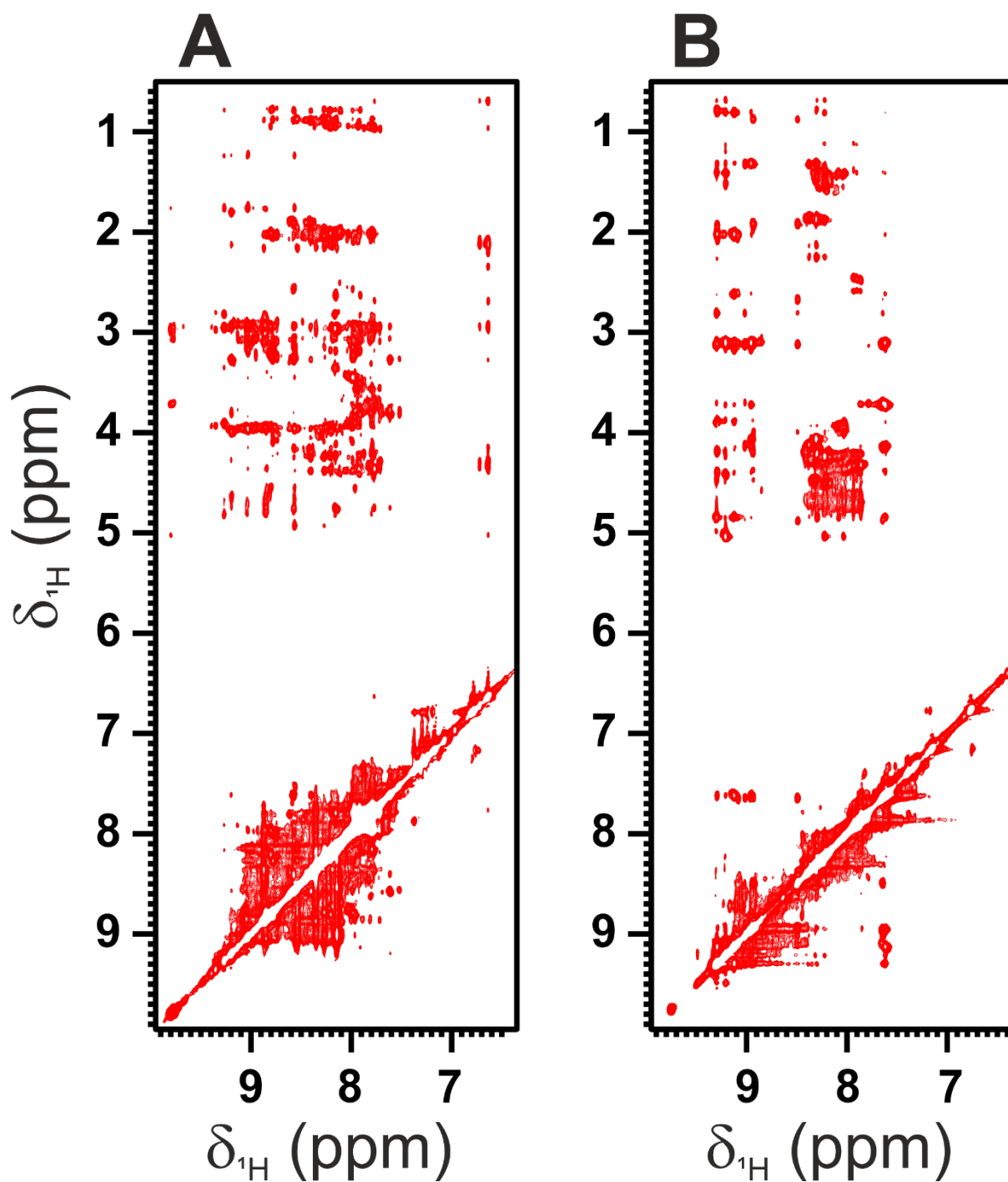


Fig. S11: H_N region of the 2D ^1H - ^1H -NOESY solution NMR spectra of A) Hook₆ and B) Hook₁₄. The spectra were recorded at 298 K on a Bruker AVANCE NEO spectrometer operating at 16.4 T (700 MHz ^1H Larmor Frequency), using water solutions (90% H_2O , 10% D_2O) of the peptides at 15 mM, in the presence of Zn(II) metal ion.

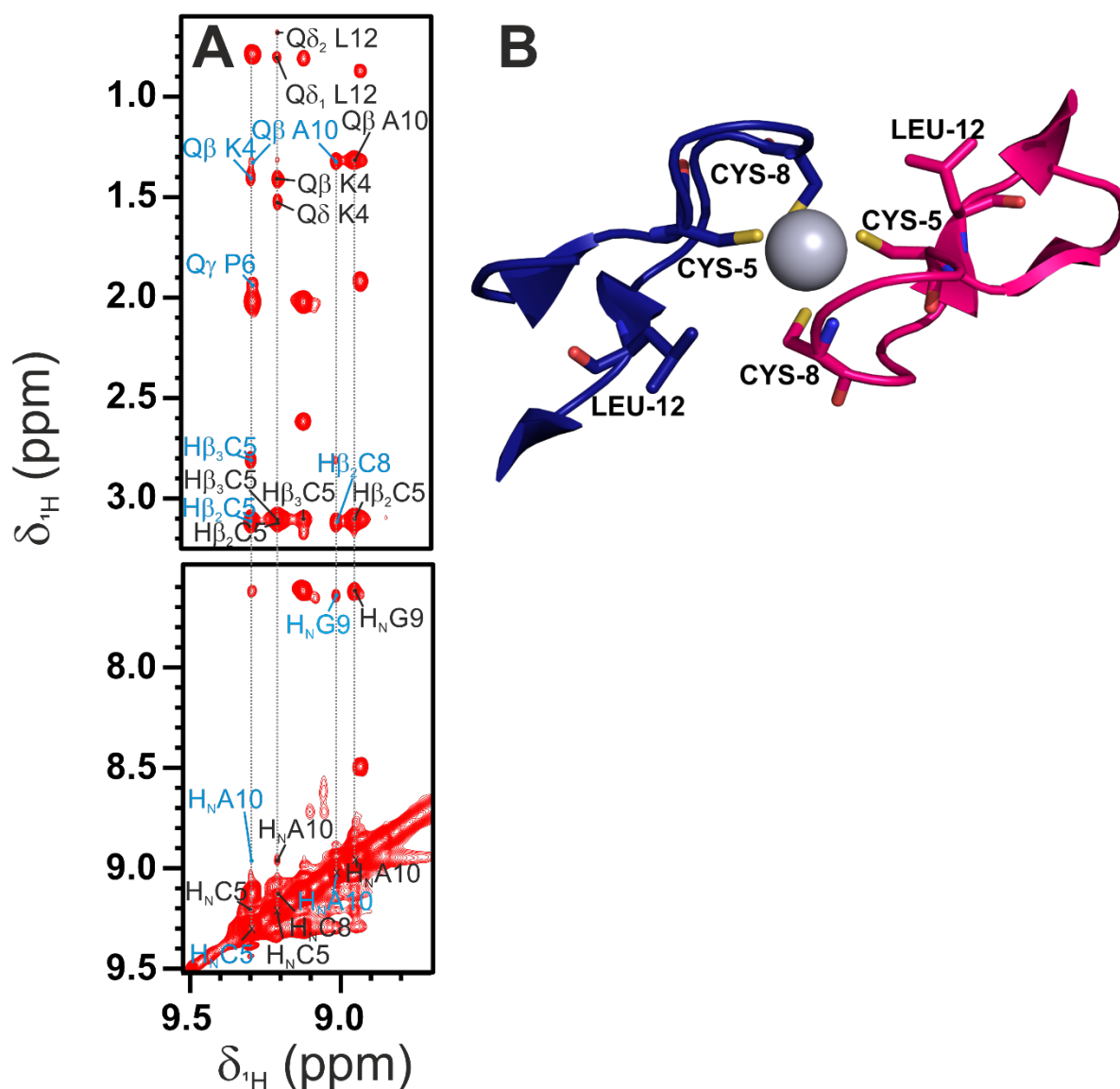


Fig. S12: (A) H_N region of the 2D ^1H - ^1H -NOESY solution NMR spectra of Hook-14 representing long-range intra- and inter-chain NOE contacts in residues C5 and C8 of both chains. The spectrum was recorded at 298 K on a Bruker AVANCE III spectrometer, operating at 22.3 T (950 MHz ^1H Larmor Frequency), using water solutions (90% H_2O , 10% D_2O) of the peptide at 15 mM, in the presence of Zn(II) metal ion. (B) Rad50 Zn-hook PDB structure (PDB code: 1L8D) indicating the position Cys-5, Cys-8 and Leu-12 in each peptide.

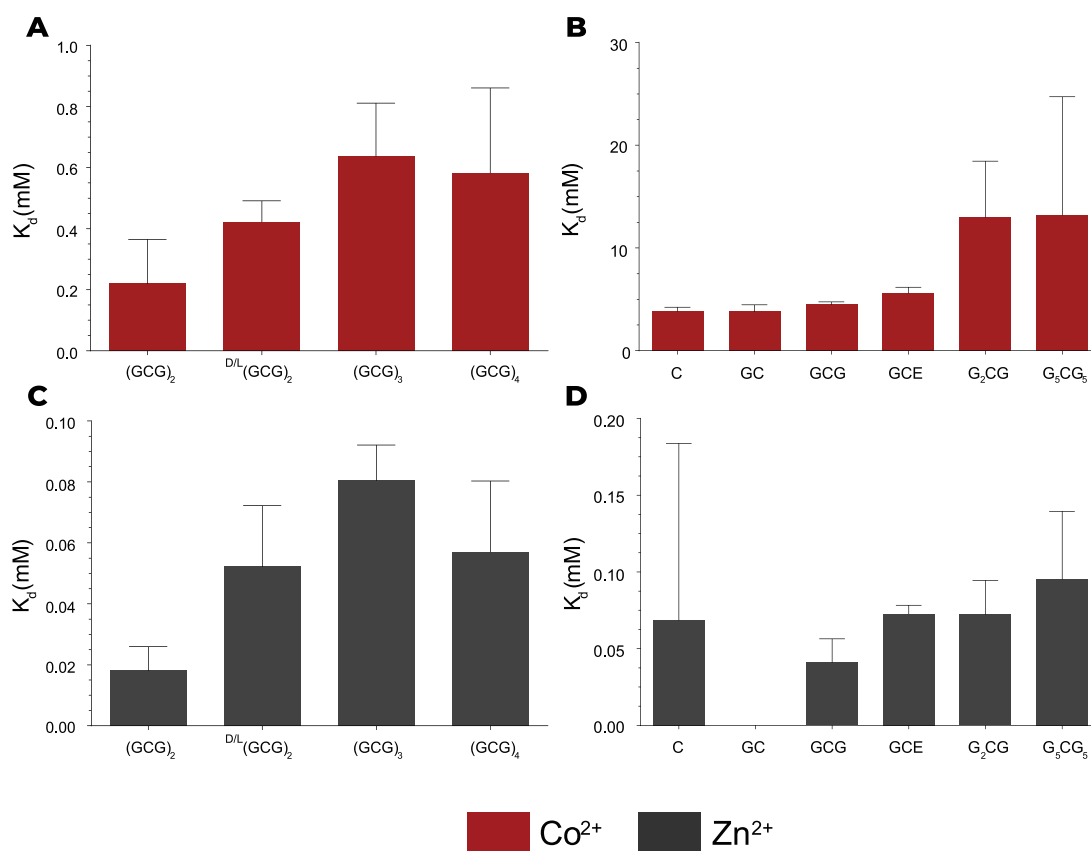


Figure S13: Dissociation constants (K_d) of a library of cysteine containing peptides for Co^{2+} (A, B) and Zn^{2+} (C, D). D/L indicates a heterochiral peptide, i.e. Gly-D-Cys-Gly-Gly-L-Cys-Gly. Data are mean \pm SD; $n = 3$.

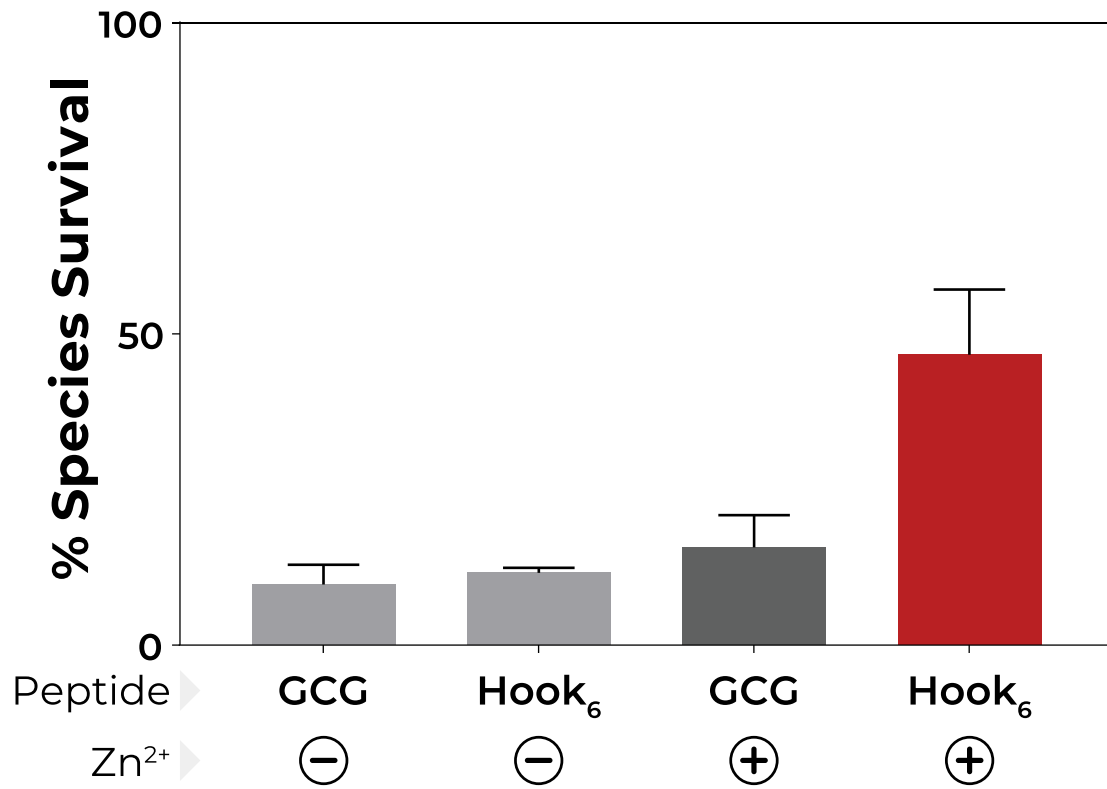


Figure S14: Competition between Hook₆ and GCG upon 16 min of UV irradiation in the presence of 1.5 mM Zn²⁺. Data are mean ±SD; n = 3.

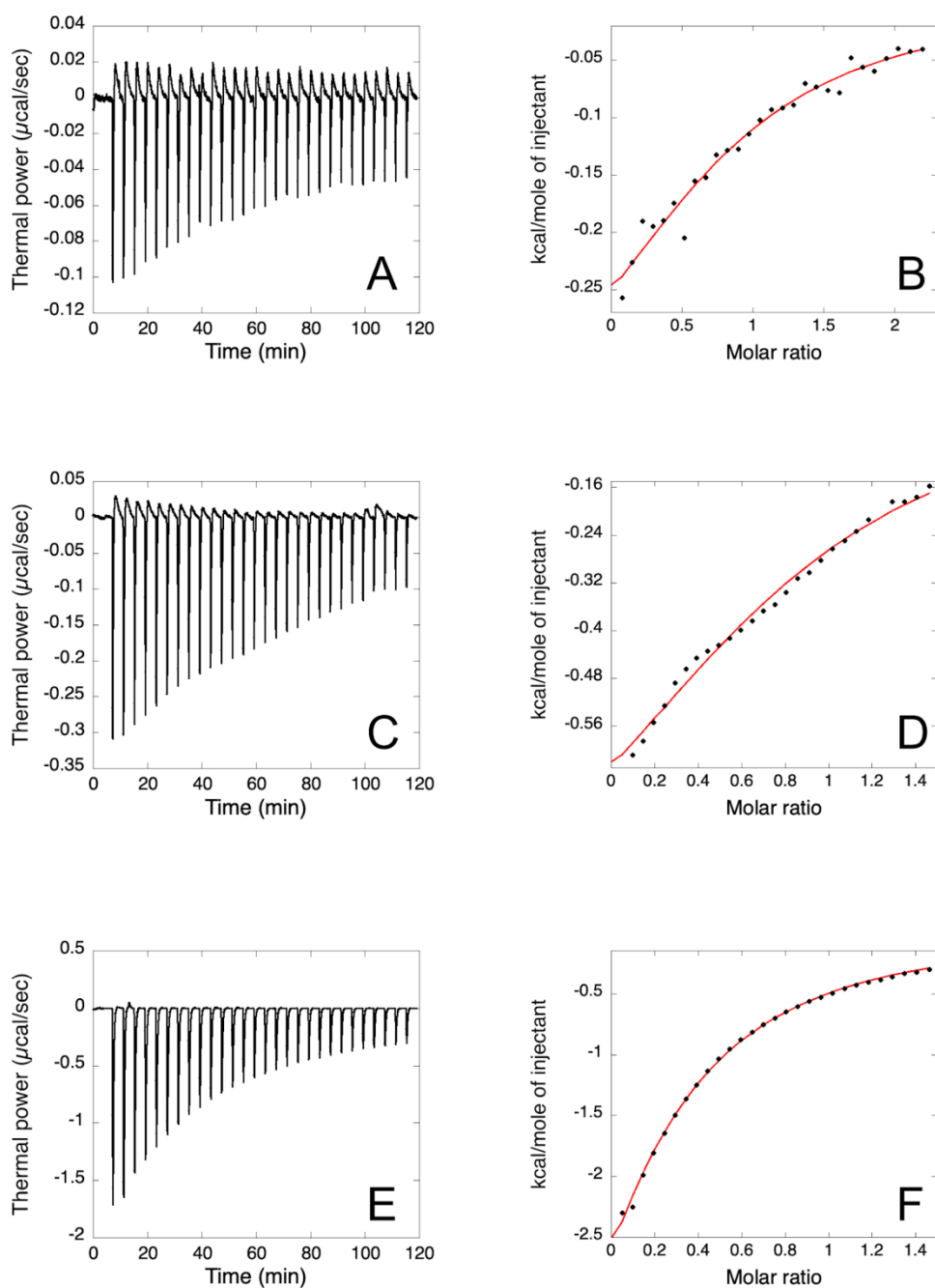


Figure S15: ITC of Zn²⁺ binding to GCG. Heat response (A, C, E) and integrated heat data as a function of the molar ratio of Zn²⁺/GCG (B, D, F) for injections of 0.75 mM (A, B), 1.0 mM (C, D), and 2.0 mM (E, F) ZnSO₄ into 75 μM, 150 μM, and 300 μM GCG, respectively. The continuous line represents the best fit of the binding isotherms, obtained with a model involving a single set of sites and “ligand in the cell” option with Origin software.

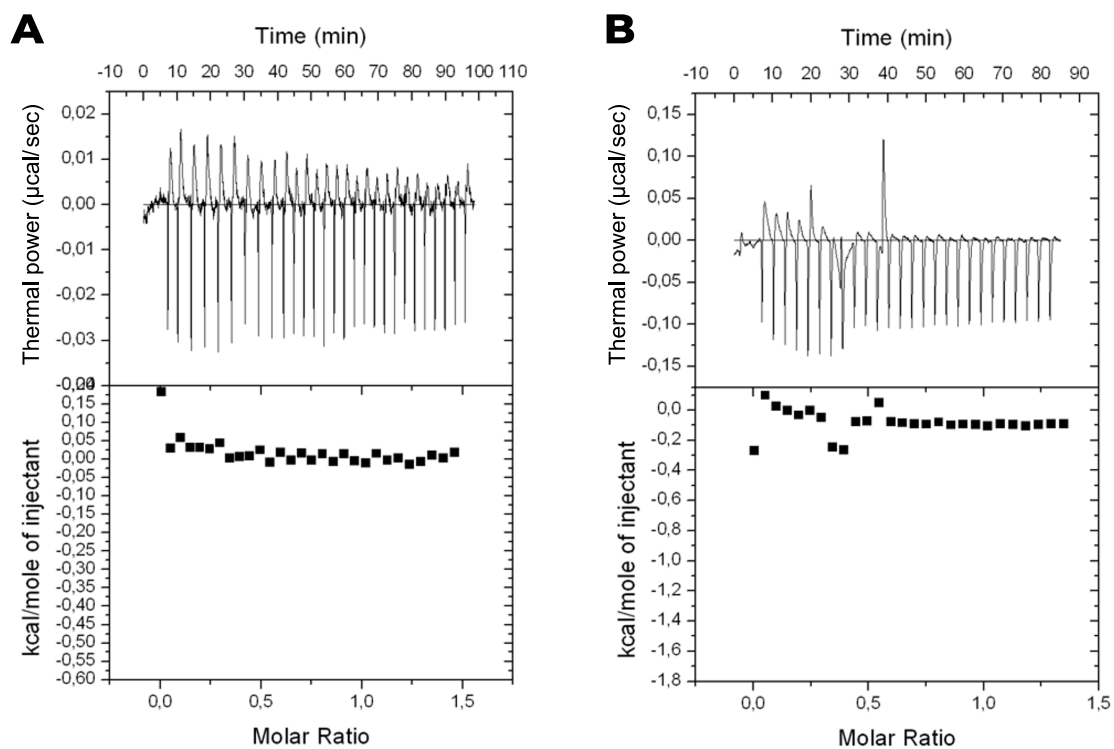


Figure S16: ITC blank control experiments. (A) Injection of 1000 μM Zn^{2+} into buffer solution in the chamber. (B) Injection of 2000 μM Zn^{2+} into buffer solution in the chamber, in absence of peptide ligand.

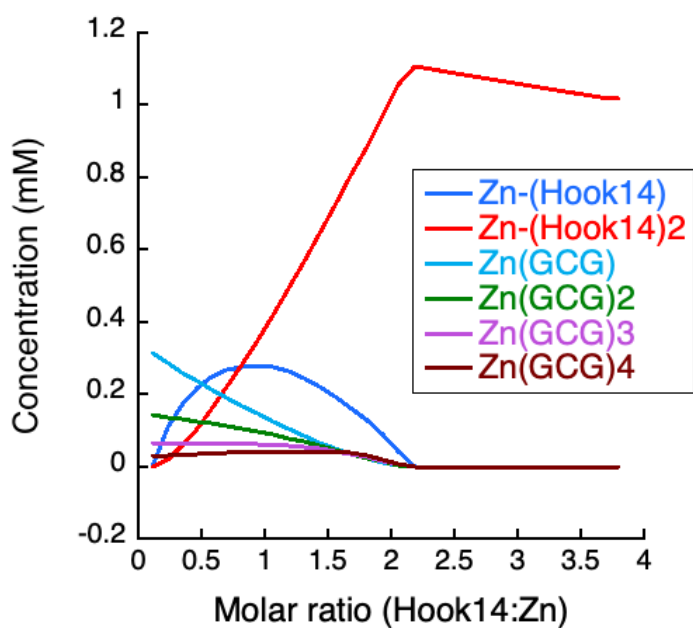


Figure S17: Affinometer simulation of Hook₁₄ peptide titrated into a solution of 1.25 mM GCG and 1.25 mM Zn^{2+} , assuming a bidentate Zn-coordination for Hook₁₄ ($K_d = 3.5$ nM) and the formation of 1:4 complex for Zn-GCG interaction ($K_d = 300$ μM).

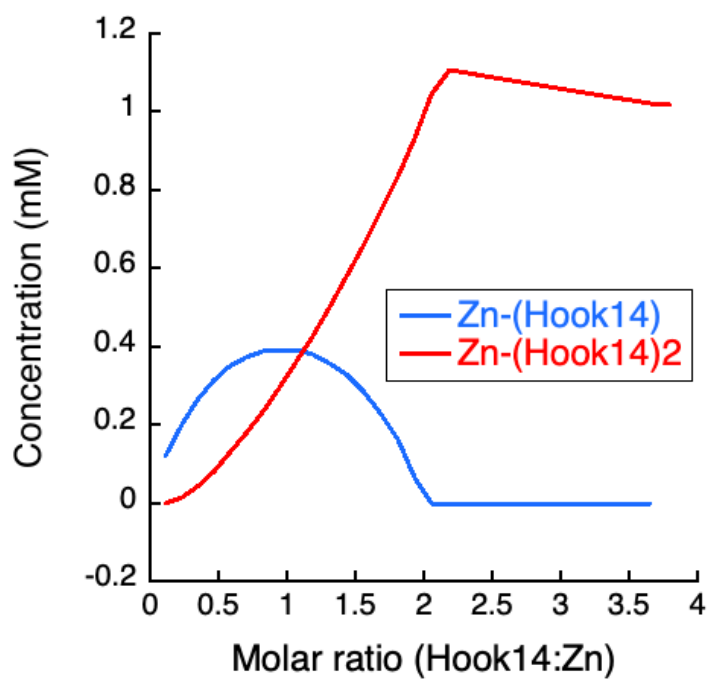


Figure S18: Affinimeter simulation of Hook₁₄ peptide titrated into a solution of 1.25 mM Zn²⁺, assuming a bidentate Zn-coordination for Hook14 ($K_d = 3.5$ nM).

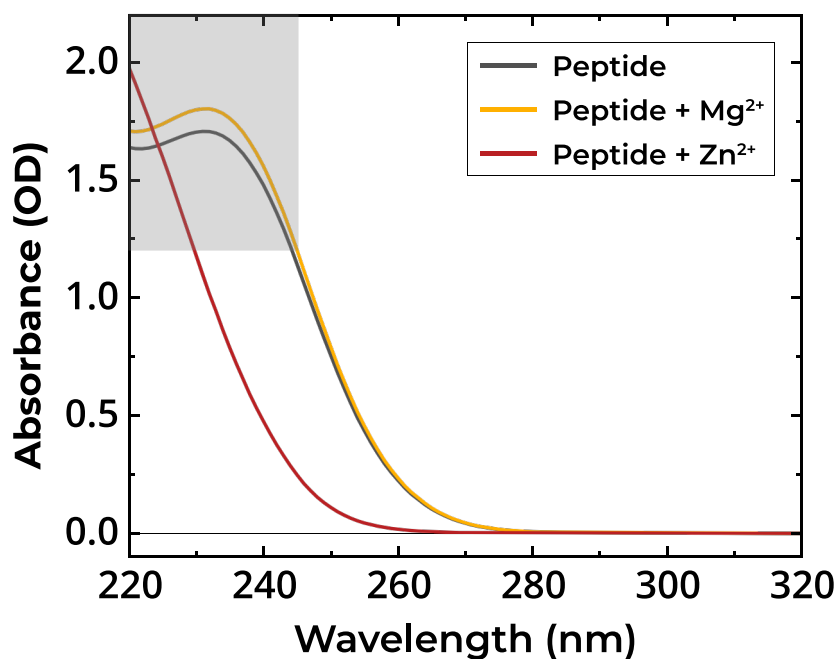


Figure S19: UV-Vis spectra of aqueous ~20 mM *N*-Acetyl Cysteine Methyl Ester in the absence of metal ions (black “peptide”, pH~9) or in presence of either ~20 mM Mg²⁺ (yellow line, pH~9) or Zn²⁺ (red line, pH~10) at an optical pathlength of 100 μm under aerobic conditions. Absorbance above 1.2 (grey shaded area) may be less accurate due to the nonlinearity of UV-Vis detection at low photon flux.

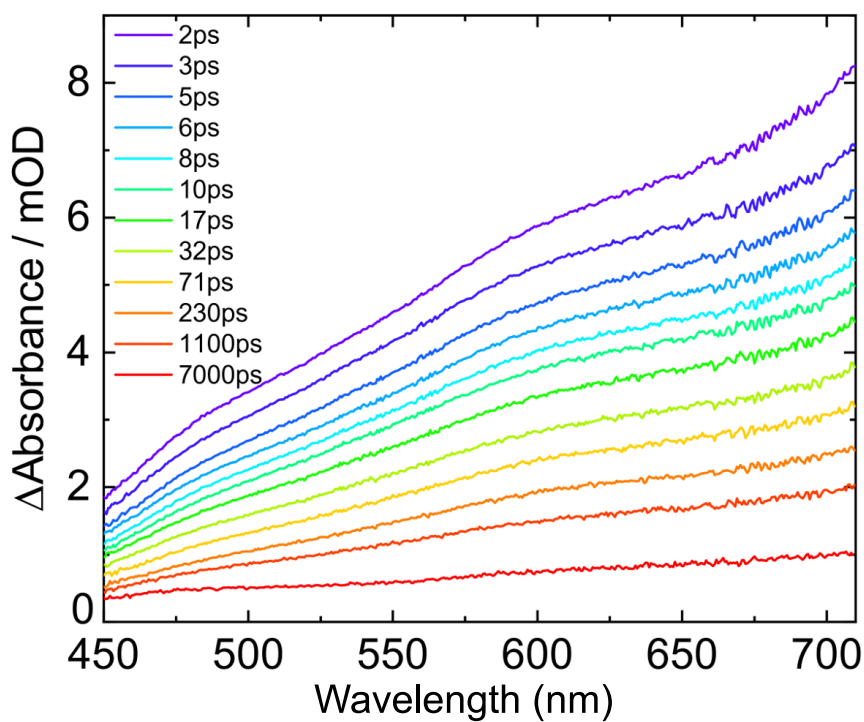


Figure S20: Absorbance difference (ΔA) spectra of *N*-Acetyl-L-cysteine methyl ester following 255 nm excitation (following horizontal lines in Figure 6B) at selected delay times between the pump and probe pulses.

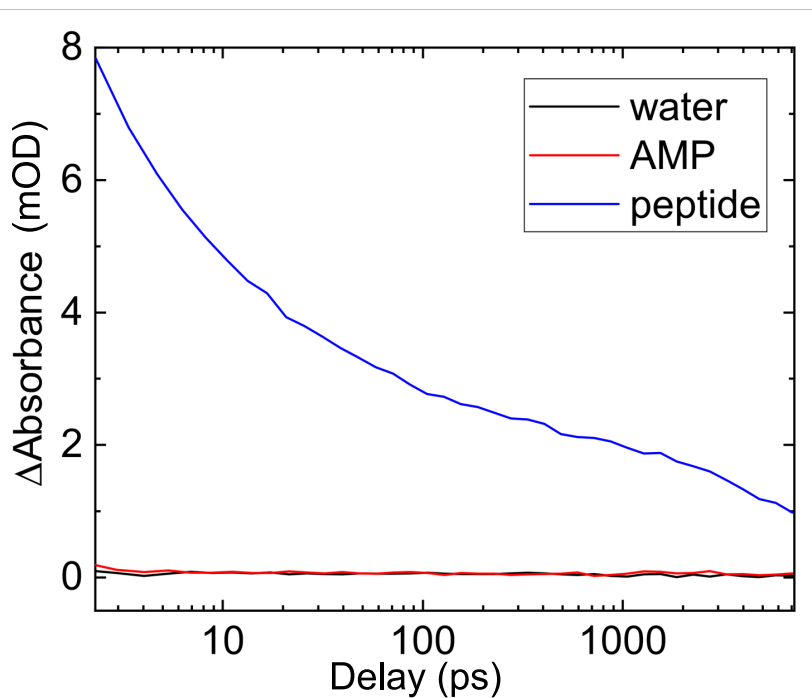


Figure S21: Absorbance difference (ΔA) signal of *N*-Acetyl-L-cysteine methyl ester (blue - “peptide”) after 255 nm excitation as a function of delay between pump and probe pulses at 700 nm (following the vertical line at 700 nm in Figure 6B). The measurement conditions were chosen carefully to minimize solvated electron production due to 2-photon-excitation of the aqueous solvent. The black line shows pure LC-MS grade water under the same excitation conditions as the sample solution. The concentration of an adenosine-monophosphate (“AMP”, Sigma Aldrich) solution was adjusted to match the absorbance of the sample solution at 255 nm (see yellow vertical line in Figure 6A) to monitor the production of solvated electrons in the presence of an equivalent absorber (red line). From these measurements, the background contribution from the solvent can be estimated to ≤ 0.1 mOD.

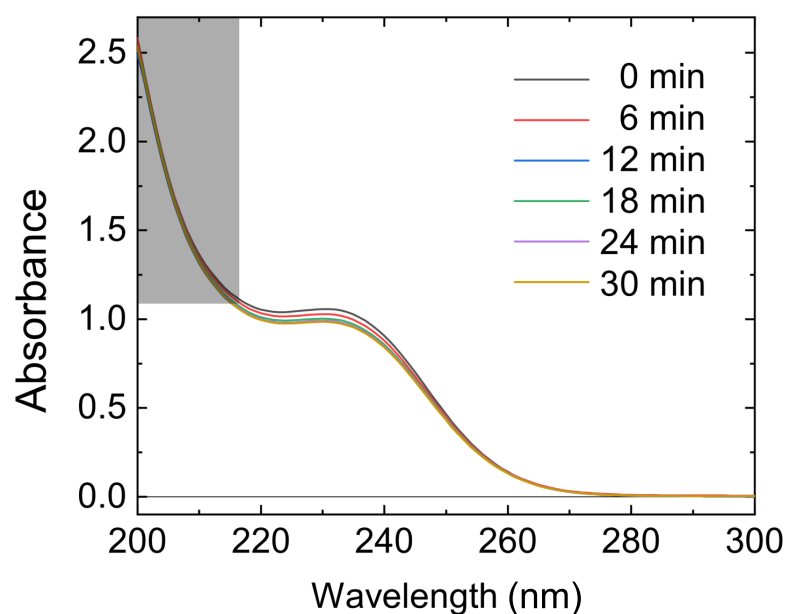


Figure S22: UV-Vis spectra of *N*-Acetyl-L-cysteine methyl ester before (0 min), during (6 min – 24 min), and after (30 min) the TA measurement (as controls of concentration and photolysis). The absorbance loss during the measurement is $\leq 7\%$ of the initial absorbance. The UV-Vis measurements were taken under aerobic conditions at an optical pathlength of 100 μm . Absorbance above ~ 1.2 (grey shaded area) may be less accurate due to the nonlinearity of UV-Vis detection at low photon flux.

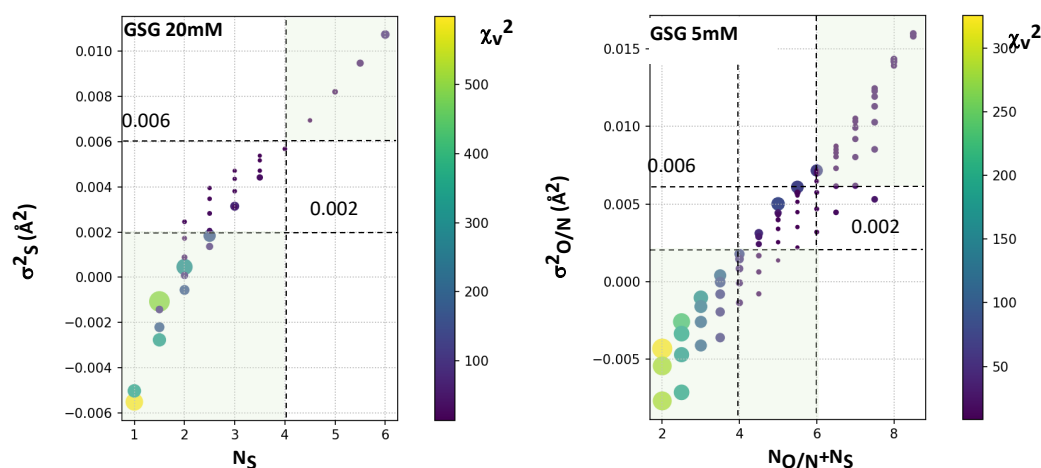
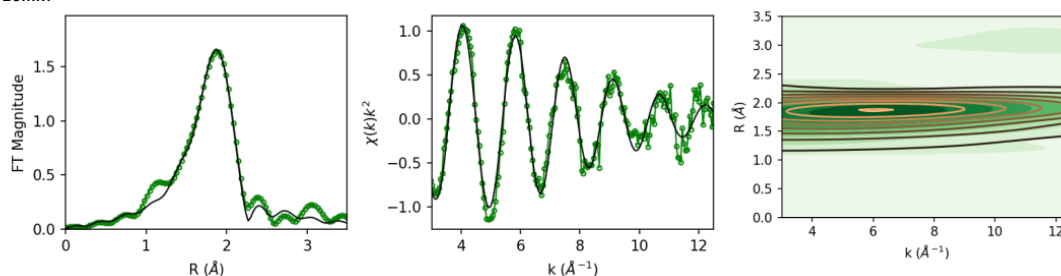


Figure S23: Analysis of EXAFS disorder parameters. A grid search of various S/N/O coordination indicates that disorder parameters below 0.002 \AA^2 lead to unreasonable low coordination number while disorder parameters above 0.006 \AA^2 lead to unreasonable total coordination numbers. Furthermore, fits having a mixed S/N/O coordination sphere show poorer results for total coordination numbers of 4 or below, as evidenced by the larger R_{factor} (circle size). Therefore, disorder parameters were limited between 0.002 and 0.006 \AA^2 , consistent with previous reports.¹⁸

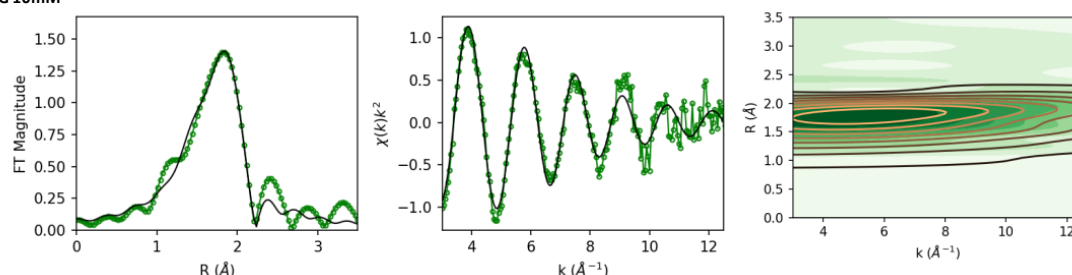
Panel S1: EXAFS fits. Multi (k^1 , k^2 , k^3)-weighted fits carried out in r -space over a k -range of 3-12.0 Å using a Hanning window (dk 1), and $S_0 = 0.9$. Bond distances and disorder parameters (Δr_{eff} and σ^2) were allowed to float having initial values of 0.0 Å and 0.003 Å² respectively, with a universal E_0 and $\Delta E_0 = 0$ eV. (σ^2 reported as $\times 10^3$ Å²). The final model fit is highlighted at the bottom of the table and plotted below. Average N/O and S coordination numbers were used for the represented (final) model using values derived from fits with an R_{FACTOR} value within 10% of the value of the best fit. These fits are also highlighted in the table.

GSG 20mM



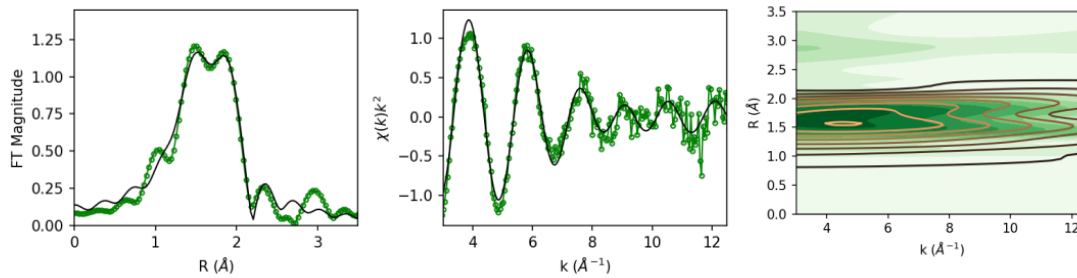
COORD. NO.		R_{FACTOR}	χ^2_{ν}	Var. No.	ΔE_0 (eV)	r (Å)	$N_{\text{N/O}}$	N_{S}	
$N_{\text{N/O}}$	N_{S}						σ^2 ($\times 10^3$ Å ²)	r (Å)	σ^2 ($\times 10^3$ Å ²)
0	4.5	0.0061	13.87	3	2.6(0.8)	-	-	2.32(0.01)	6.9(0.5)
0	4	0.0064	14.67	3	2.7(0.8)	-	-	2.32(0.01)	5.7(0.4)
1.5	3.5	0.0049	18.99	5	5.1(2.)	2.12(0.05)	11.7(11.9)	2.33(0.01)	5.4(1.0)
1	3.5	0.0052	20.10	5	4.4(1.8)	2.09(0.06)	8.3(9.4)	2.33(0.01)	5.2(0.8)
2	3	0.0053	20.43	5	6.8(2.)	2.13(0.03)	8.1(5.8)	2.34(0.01)	4.7(1.1)
1.5	3	0.0056	21.87	5	6.(1.7)	2.10(0.04)	5.8(4.7)	2.34(0.01)	4.4(0.8)
0.5	3.5	0.0057	22.05	5	3.8(1.4)	2.05(0.06)	1.3(5.3)	2.33(0.01)	4.7(0.6)
2.5	2.5	0.0058	22.53	5	8.6(2.)	2.14(0.03)	6.4(3.7)	2.35(0.01)	4.0(1.2)
2	2.5	0.0062	24.27	5	7.7(1.8)	2.12(0.03)	4.5(3.1)	2.35(0.01)	3.5(1.0)
0	4	0.0064	14.67	3	2.7(0.8)	-	-	2.32(0.01)	5.7(0.4)

GSG 10mM



COORD. NO.		R_{FACTOR}	χ^2_{ν}	Var. No.	ΔE_0 (eV)	r (Å)	$N_{\text{N/O}}$	N_{S}	
$N_{\text{N/O}}$	N_{S}						σ^2 ($\times 10^3$ Å ²)	r (Å)	σ^2 ($\times 10^3$ Å ²)
1.5	3.5	0.0060	17.71	5	-1.7(1.8)	2.02(0.05)	6.7(3.4)	2.31(0.01)	5.8(0.8)
2	3	0.0061	18.29	5	-0.5(1.8)	2.04(0.04)	6.8(2.7)	2.32(0.01)	4.9(0.9)
2.5	2.5	0.0065	19.36	5	1.0(1.8)	2.06(0.03)	6.4(2.2)	2.33(0.01)	3.9(0.9)
3	2	0.0069	20.54	5	2.6(1.8)	2.08(0.03)	5.9(1.8)	2.34(0.01)	2.7(1.0)
1.5	3	0.0076	22.50	5	-0.7(1.7)	2.03(0.03)	3.2(2.5)	2.32(0.01)	4.5(0.8)
2	2.5	0.0082	24.27	5	0.7(1.8)	2.05(0.03)	3.6(2.1)	2.33(0.01)	3.4(0.9)
2.5	2	0.0089	26.40	5	2.3(1.8)	2.07(0.03)	3.6(1.8)	2.34(0.01)	2.2(1.0)
2.3(0.6)	2.8(0.6)	0.0061	18.19	5	0.1(1.9)	2.05(0.04)	7.3(2.5)	2.32(0.01)	4.5(0.8)

GSG 5mM



COORD. NO.		R _{FACTOR}	X ² _v	Var. No.	ΔE ₀ (eV)	r(Å)	N _{N/O}		N _S	
N _{N/O}	N _S						σ ² (x10 ³ Å ²)	r(Å)	σ ² (x10 ³ Å ²)	
3.5	2	0.0056	8.92	5	-2.0(1.4)	2.01(0.02)	5.1(1.2)	2.31(0.01)	3.1(0.8)	
3	2.5	0.0057	8.96	5	-3.0(1.4)	1.99(0.02)	4.5(1.3)	2.31(0.01)	4.6(0.8)	
2.5	3	0.0057	9.00	5	-3.8(1.4)	1.98(0.02)	3.5(1.3)	2.30(0.01)	5.8(0.8)	
2.5	2.5	0.0058	9.23	5	-3.2(1.3)	1.99(0.02)	2.5(1.2)	2.30(0.01)	4.1(0.8)	
4	2	0.0065	10.33	5	-1.8(1.6)	2.01(0.02)	6.9(1.4)	2.32(0.01)	3.6(1.0)	
3	2	0.0066	10.47	5	-2.2(1.4)	2.00(0.02)	3.4(1.2)	2.31(0.01)	2.6(0.8)	
3.5	2.5	0.0073	11.50	5	-2.8(1.7)	2.00(0.02)	6.5(1.6)	2.31(0.01)	5.1(1.1)	
3.5	2.5	0.0073	11.50	5	-2.8(1.7)	2.00(0.02)	6.5(1.6)	2.31(0.01)	5.1(1.1)	
2.5	2	0.0108	17.19	5	-2.4(1.7)	2.00(0.02)	1.7(1.4)	2.31(0.01)	2.2(1.0)	
3.1(0.6)	2.4(0.4)	0.0056	8.93	5	-2.8(1.3)	2.00(0.02)	4.6(1.2)	2.31(0.01)	4.3(0.8)	

Table S1: Peptides used in this work and K_d values for Co^{2+} and Zn^{2+} calculated by direct or competitive titration experiments, respectively.

	$K_d \text{ Co}^{2+}$ (mM)	$K_d \text{ Zn}^{2+}$ (mM)
GCG	4.5 ± 0.2	0.041 ± 0.015
(GCG) ₂	0.18 ± 0.11	0.018 ± 0.008
(GCG) ₃	4.5 ± 0.2	0.081 ± 0.012
(GCG) ₄	0.22 ± 0.11	0.057 ± 0.023
^{D/L} (GCG) ₂	0.64 ± 0.12	0.052 ± 0.02
Hook ₆ (KCPVCG)	0.19 ± 0.04	0.0029 ± 0.0027
Hook ₁₄ (AKGKCPVCGAELTD) ²	0.065 ± 0.002	$3.54\text{E-}6$

Table S2: Parameters calculated from ITC investigation of GCG peptide.

	75 μM	150 μM	300 μM
K_a (M^{-1})	$1.67\text{E}4 \pm 3.26\text{E}3$	$1.02\text{E}4 \pm 2.30\text{E}3$	$1.34\text{E}3 \pm 228$
K_d (μM)	60 ± 12	98 ± 22	746 ± 127
ΔH (cal/mol)	-378.8 ± 27.45	-920.3 ± 51.24	2075 ± 39.44
ΔS (cal/mol*K)	18.0	15.3	7.35
N	1.17 ± 0.15	1.11 ± 0.06	4.21 ± 0.46

Table S3: Vertical excitations energies (in eV) of the model peptide coordinating Zn^{2+} cations, obtained at the ADC(2)/TZVP level of theory, assuming the ground-state minimum-energy geometry found using the CAM-B3LYPD3BJ/def2-TZVP method.

State / Transition	Molecule name	$E_{\text{exc}}/(\text{eV})$	f_{osc}	$\lambda/(\text{nm})$
S ₁	$n_s\pi^*(\text{CT})$	5.64	0.006	220
S ₂	$n_s\pi^*(\text{CT})$	5.76	0.010	215
S ₃	$n\pi^*$	5.92	0.000	209
S ₄	$n\pi^*$	6.09	0.001	204
S ₅	$n_s\sigma^*(\text{CT})$	6.21	0.025	200
S ₆	$n_s\pi^*(\text{CT})$	6.29	0.047	197
S ₇	$n\pi^*$	6.41	0.151	193
S ₈	$n_s\pi^*(\text{CT})$	6.67	0.167	186

Table S4: Vertical excitations energies (in eV) of the model peptide with one explicit water molecule, obtained at the ADC(2)/TZVP level of theory including the COSMO solvent model of bulk water and assuming the ground-state minimum-energy geometry found using the CAM-B3LYP-D3BJ/def2-TZVP method.

State / Transition	Molecule name	$E_{exc}/(eV)$	fosc	$\lambda/(nm)$
S ₁	$n_S\pi^*(CT)$	5.48	0.006	226
S ₂	$n_S\pi^*(CT)$	5.54	0.003	224
S ₃	$n\pi^*$	5.96	0.001	208
S ₄	$n\pi^*$	6.00	0.000	207
S ₅	$n\pi^*$	6.03	0.001	206
S ₆	$n_S\pi^*(CT)$	6.12	0.008	203
S ₇	$n_S\pi^*(CT)$	6.21	0.068	200
S ₈	$n\pi^*$	6.46	0.002	192

Supplementary references

- 1 C. Bonfio, L. Valer, S. Scintilla, S. Shah, D. J. Evans, L. Jin, J. W. Szostak, D. D. Sasselov, J. D. Sutherland and S. S. Mansy, *Nat. Chem.*, 2017, **9**, 1229–1234.
- 2 T. Kočańczyk, P. Jakimowicz and A. Krężel, *Chem. Comm.*, 2013, **49**, 1312–1314.
- 3 H. C. Cheng, *J. Pharmacol. Toxicol. Methods.*, 2001, **46**, 61–71.
- 4 S. Keller, C. Vargas, H. Zhao, G. Piszczek, C. A. Brautigam and P. Schuck, *Anal. Chem.*, 2012, **84**, 5066–5073.
- 5 B. Ravel and M. Newville, *J. Synchrotron Radiat.*, 2005, **12**, 537–541.
- 6 M. Newville, *J. Phys. Conf. Ser.*, 2013, **430**, 12007.
- 7 M. Newville, *J. Synchrotron. Radiat.*, 2001, **8**, 96–100.
- 8 J. J. Rehr and R. C. Albers, *Rev. Mod. Phys.*, 2000, **72**, 621–654.
- 9 P. Bevington and D. K. Robinson, *Data Reduction and Error Analysis for the Physical Sciences*, McGraw-Hill Education, 2003.
- 10 M. Barbatti, A. C. Borin and S. Ullrich, *Top Curr. Chem.*, 2015, **355**, 1–32.
- 11 G. Schaftenaar, E. Vlieg and G. Vriend, *J. Comput. Aided. Mol. Des.*, 2017, **31**, 789–800.
- 12 M. D. Hanwell, D. E. Curtis, D. C. Lonie, T. Vandermeersch, E. Zurek and G. R. Hutchison, *J. Cheminform.*, 2012, **4**, 17.

- 13 T. Yanai, D. P. Tew and N. C. Handy, *Chem. Phys. Lett.*, 2004, **393**, 51–57.
- 14 F. Neese, F. Wennmohs, A. Hansen and U. Becker, *Chem. Phys.*, 2009, **356**, 98–109.
- 15 C. Hättig, in *Adv. Quantum Chem.*, ed. H. J. Å. Jensen, Academic Press, 2005, vol. 50, 37–60.
- 16 A. Dreuw and M. Wormit, *WIREs Comput. Mol. Sci.*, 2015, **5**, 82–95.
- 17 S. Karbalaei Khani, A. Marefat Khah and C. Hättig, *Phys. Chem. Chem. Phys.*, 2018, **20**, 16354–16363.
- 18 K. Clark-Baldwin, D. L. Tierney, N. Govindaswamy, E. S. Gruff, C. Kim, J. Berg, S. A. Koch and J. E. Penner-Hahn, *J. Am. Chem. Soc.*, 1998, **120**, 8401–8409.